PHILOSOPHICAL TRANSACTIONS A

royalsocietypublishing.org/journal/rsta

Research

Cite this article: Sedov V *et al*. 2023 Narrowband photoluminescence of Tin-Vacancy colour centres in Sn-doped chemical vapour deposition diamond microcrystals. *Phil. Trans. R. Soc. A* **382**: 20230167.
https://doi.org/10.1098/rsta.2023.0167

Received: 17 April 2023
Accepted: 20 July 2023

One contribution of 9 to a Theo Murphy meeting issue 'Diamond for quantum applications'.

Subject Areas:
solid-state physics, materials science, spectroscopy

Keywords:
diamond, colour centres, Tin-Vacancy, CVD, spectroscopy

Author for correspondence:
Vadim Sedov
e-mail: sedovvadim@yandex.ru

Electronic supplementary material is available online at https://doi.org/10.6084/m9.figshare.c.6908883.

Narrowband photoluminescence of Tin-Vacancy colour centres in Sn-doped chemical vapour deposition diamond microcrystals

Vadim Sedov[1], Artem Martyanov[1], Arthur Neliubov[2,3], Ivan Tiazhelov[1], Sergey Savin[4], Ivan Eremchev[5], Maksim Eremchev[3,5], Margarita Pavlenko[5,6], Soumen Mandal[7], Victor Ralchenko[1,8] and Andrei Naumov[3,5,9]

[1]Prokhorov General Physics Institute of the Russian Academy of Sciences, Vavilov Street 38, Moscow 119991, Russia
[2]Center for Engineering Physics, Skolkovo Institute Science and Technology, Nobel Street, Building 1, Moscow 121205, Russia
[3]Lebedev Physical Institute of the Russian Academy of Sciences, Troitsk, Moscow 108840, Russia
[4]MIREA - Russian Technological University, Prospect Vernadskogo 78, Moscow 119454, Russia
[5]Moscow Pedagogical State University, Moscow 119435, Russia
[6]National Research University Higher School of Economics, Moscow 109028, Russia
[7]School of Physics and Astronomy, Cardiff University, Queen's Buildings, The Parade, Cardiff, UK
[8]Harbin Institute of Technology, 92 Xidazhi Street, Harbin 150001, People's Republic of China
[9]Institute of Spectroscopy RAS, Troitsk, Moscow 108840, Russia

VS, 0000-0001-9802-1106; AM, 0000-0002-3196-5695; AN, 0000-0002-3110-2902; IT, 0000-0002-6893-2918; SS, 0000-0003-0350-0847; IE, 0000-0002-2239-5176; ME, 0000-0003-2336-1637; MP, 0009-0009-9183-0643; SM, 0000-0001-8912-1439; VR, 0000-0002-2213-4224; AN, 0000-0001-7938-9802

THE ROYAL SOCIETY PUBLISHING

Tin-Vacancy (Sn-V) colour centres in diamond have a spin coherence time in the millisecond range at temperatures of 2 K, so they are promising to be used in diamond-based quantum optical devices. However, the incorporation of large Sn atoms into a dense diamond lattice is a non-trivial problem. The objective of our work is to use microwave plasma-assisted chemical vapour deposition (CVD) to grow Sn-doped diamond with submicron SnO_2 particles as a solid-state source of impurity. Well-faceted diamond microcrystals with sizes of a few micrometres were formed on AlN substrates. The photoluminescence (PL) signal with zero-phonon line (ZPL) peak for Sn-V centre at ≈620 nm was measured at room temperature (RT) and at 7 K. The peak width (full width at half-maximum) was measured to be 1.1–1.7 nm at RT and ≈0.05 nm at 7 K. The observed variations of ZPL shape and position, in particular, narrowing of PL peak at RT and formation of single-line fine structure at low-*T*, are attributed to strain in the crystallites. The diamond doping with Sn via CVD process offers a new route to from Sn-V colour centre in the bulk of the diamond crystallites.

This article is part of the Theo Murphy meeting issue 'Diamond for quantum applications'.

1. Introduction

Group-IV colour centres in diamond like Silicon-Vacancy (Si-V), Germanium-Vacancy (Ge-V) and Tin-Vacancy (Sn-V) possess narrowband photoluminescence (PL) emission at room temperature (RT) in the visible or near-IR spectral ranges and, thus, attract significant attention due to their possible applications in quantum information technologies [1–6], biomedicine (optical biomarkers and drug carriers) [7–9] and local optical thermometry [10–13]. Regarding quantum information applications, Sn-V is predicted to be the most suitable out of the listed Group-IV colour centres. The larger atomic radii of Sn leads to higher splitting in ground state and therefore spin-level structure can be resolved at higher temperature (approx. 2 K) with spin coherence time in the millisecond range [1,14]. This is less expensive in comparison with Si-V and Ge-V centres, which require sub-Kelvin regimes of operation [15]. Operating in a 2–5 K temperature range leads to a significant decrease in spin coherence times down to sub-microsecond in the case of Si-V and Ge-V [16,17]. Thus, reliable methods for the controlled formation of Sn-V centres in diamond are required.

The most prevalent of all Group-IV centres, the Si-V centre was known since the dawn of the era of lab-grown diamond in the early 1980s [18]. However, similar in structure Ge-V and Sn-V centres were both discovered less than a decade ago [15,19–23]. One of the reasons is the big size of germanium and tin atoms, which makes it a lot more difficult to be incorporated into the dense diamond lattice. The second obstacle is the Ge-C and Sn-C bonds, which are much weaker than C–C bonds, thus inhibiting the process of diamond doping [22]. Therefore, the first samples with Ge-V and Sn-V centres in diamond were obtained by using ion implantation [15,19]. Using ion implantation, the desired concentrations of the selected dopant along with the choice of the isotope content of the impurity is possible. The major downsides of the ion implantation are (i) collateral lattice damage [24] that is not fully compensated even after vacuum and high-pressure high-temperature (HPHT) annealing; (ii) the limitation on the implantation depth, so only the near-surface layer can be doped; and (iii) the lack of possibility to form bulk material with a universal distribution of impurity. In addition, for diamond, the excess concentration of the implanted ions may lead to the graphitization of the substrate [25].

Alternatively, Ge-doped diamond may be obtained using HPHT synthesis or chemical vapour deposition (CVD) [21,23,26,27]. However, the incorporation of Sn atoms into diamond is a non-trivial problem. The Sn-doped HPHT diamonds are limited in size to submillimetre crystals [22,28]. On the other hand, the CVD method, used for doping with Si and Ge, is still undeveloped for Sn doping. In the past, Sn-doped submicron crystals and epitaxial film were grown in microwave plasma using a mixture of SnO_2 and $SnCl_2$ particles as dopant source [29]. To the best of our knowledge that is the only experiment in the literature; however, the low spectral

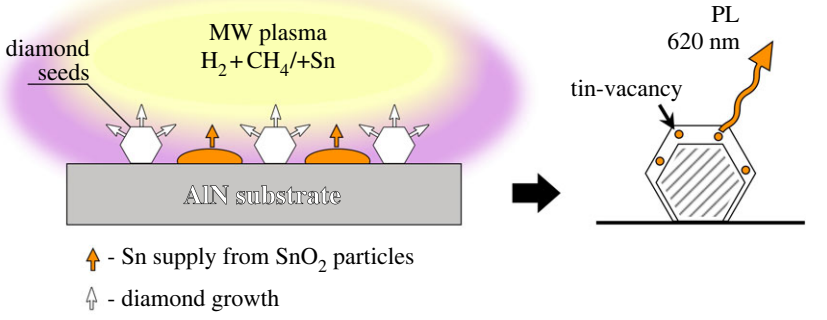

Figure 1. Scheme of the experiment.

quality of the resulting material made it unsuitable for quantum applications. Consequently, the current-state-of-the-art for using Sn-V centres for quantum applications is heavily dependent on implanted material [14,30–33].

In this work, we report on the formation of Sn-V centres in the CVD-grown high-quality diamond by using tin oxide nanoparticles as a solid-state source of impurity. The grown microcrystals exhibit narrowband luminescence with zero-phonon line (ZPL) near 620 nm, which is attributed to the emission of the formed Sn-V centres. The statistical characterization of the stress and luminescent characteristics (both at RT and at 7 K) of different microcrystals is performed.

2. Methods

The schematic of the experimental growth method is shown in figure 1. The Sn-doped diamond layers are deposited using MW CVD in methane–hydrogen gas mixtures. During the growth process, solid-state Sn-containing particles are placed near the diamond seeds to serve as the source of impurity during growth. Throughout the process, Sn atoms which are etched by atomic hydrogen, are incorporated into the diamond lattice, forming luminescent Sn-V centres.

The polycrystalline polished AlN plates with sizes of $10 \times 10 \times 1\,\mathrm{mm}^3$ were chosen as substrates in order to avoid any interference from self-doping from the substrate material (for example, Si in the case of silicon substrates) [27,34]. Prior to deposition, the substrates were sequentially seeded in water-based slurries: first, with SnO_2 nanoparticles (size 90–300 nm, $10\,\mathrm{mg\,ml}^{-1}$), and then with submicrometre HPHT diamond particles (size 250–500 nm, SYNDIA VANMOPPES, SYP series, $0.3\,\mathrm{mg\,ml}^{-1}$).

The diamond layers were deposited using ARDIS-100 (2.45 GHz, Optosystems Ltd, Russia) [35,36] CVD system with the following process parameters: the total gas flow of 500 sccm, the methane concentration of 4%, the gas pressure of 75 Torr and the microwave power 4.5 kW. The substrate temperature was kept at 980°C as measured with the two-colour pyrometer METIS M322 (SensorTherm GmbH). The deposition time was 20 min.

The process of Sn incorporation in diamond is thought to follow a mechanism similar to incorporation of Si and Ge atoms in diamond from respective solid precursor [20,34,37]. First, the Si (Ge) crystal is etched by atomic hydrogen to form volatile SiH_x (or GeH_x) products, which admix with CH_4–H_4 plasma, then are adsorbed on the diamond surface, and eventually incorporated in the diamond lattice occupying an interstitial position. Following a similar pathway, the reaction chain for SnO_2 etching can be described as SnO_2 (solid) → SnO → Sn → SnH_x (gas). The melting point (T_m) of SnO_2 is 1630°C and that of SnO and Sn are 1040°C and 231.9°C, respectively, which is lower than the melting point of the starting material.

For selective removal of the remaining Sn-containing particles, the as-grown samples were treated in a mixture of concentrated acids, $HF:HNO_3$ (1 : 1, 99% pure, 1 min). The surface

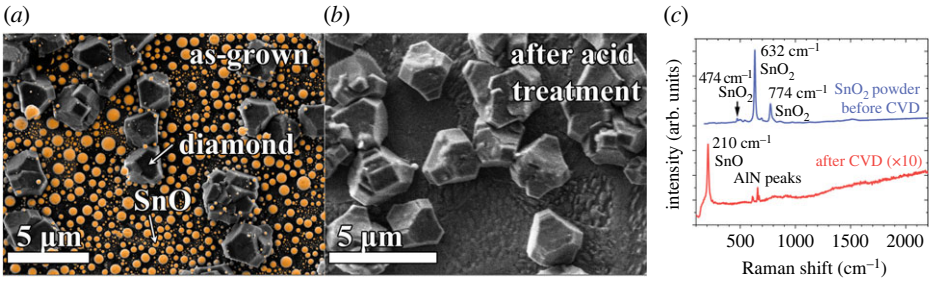

Figure 2. SEM images of the as-grown diamond microparticles on AlN substrates before (*a*) and after (*b*) acid treatment performed to remove Sn-containing particles (small ball-shaped particles coloured orange). (*c*) Raman spectra of Sn-containing particles before and after CVD growth.

morphology of the samples and crystal sizes were examined using a Tescan MIRA3 scanning electron microscope (SEM), equipped with an energy-dispersive X-ray spectroscopy (EDX) module for elemental analysis. Raman and PL spectra at RT were taken with a LabRam HR840 (Horiba) spectrometer in a confocal configuration. The laser beam of 473 nm wavelength was focused to a ≈1 µm spot on the sample surface on different locations (Olympus BX41).

For low-temperature measurements, PL spectra were measured with a custom-built fluorescence microscope. In brief, continuous-wave tuneable laser OPO C-Wave (Hubner Photonics) was used as an excitation source. However, in the spectral region near ZPL of Sn-V centres (≈620 nm), the laser's wavelength could not be tuned continuously, which prevented us from the reliable investigation of photoluminescence excitation (PLE) spectra. Thus, the laser wavelength was set to the most effective excitation region from the a_{2u} state in the valence band [31] and in most experiments was 543 nm. The sample was placed in a closed-cycle He^4 cryocooler CS204SF-DMX-20 (ARS). The temperature was controlled by Lakeshore 335. Emission from single microcrystal was collected with 50X Mitutoyo Plan Apo SL objective (NA = 0.42) and spectrally analysed with SOL Instruments spectrometer MS5204i equipped with a cooled CCD camera (QE > 90% near 620 nm). The spectral resolution was 0.033 nm for the investigated spectral region.

3. Results

(a) Synthesis and structure of Sn-doped diamond microcrystals

The SEM images of the surface of the as-grown sample are shown in figure 2. After the growth, diamond seeds evolved in a set of individual well-faceted microcrystals with sizes in the range of 2–4 µm and the shape typical for high-quality non-twinned diamond [38]. Near the crystals, plenty of submicron spherical-shaped Sn-containing particles were also found (figure 2*a*—coloured in orange using the method described in [39]). The Sn-based particles are sprinkled mostly between the diamond crystallites. Some smaller metal-based particles can be seen sitting on diamond facets, which can be ascribed to redeposition of the Sn compound. Those Sn-containing particles can be selectively removed by acid treatment (figure 2*b*). The comparison of the Raman spectra of the SnO_2 particles and the resulting Sn-containing diamond particles after the CVD process is shown in figure 2*c*. The powder SnO_2 spectrum shows a set of typical SnO_2 peaks at 474, 632 and 774 cm^{-1} [40]. The spectrum of the particles after the CVD process did not have any of the SnO_2 peaks. However, a new peak appears at 210 cm^{-1}, which is the A_{1g} mode of suboxide SnO [41], indicating a reduction of tin(IV) oxide to tin(II) oxide in the plasma environment with atomic hydrogen abundance. The fact that we still observe tin-containing particles after 20 min of the CVD process is evidence of the absence of the intensive sublimation or plasma-chemical reaction. This opens up the possibility to use SnO_2 particles as the solid-state dopant source for prolonged diamond growth runs.

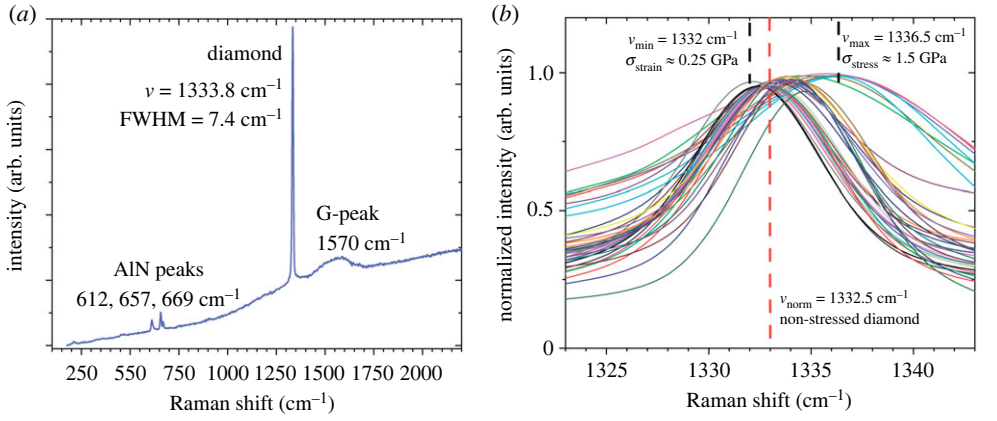

Figure 3. Raman spectra of the as-grown diamond microcrystal (*a*) and the combined normalized statistics of the Raman lines of the diamond phase over 40 investigated microcrystals (*b*).

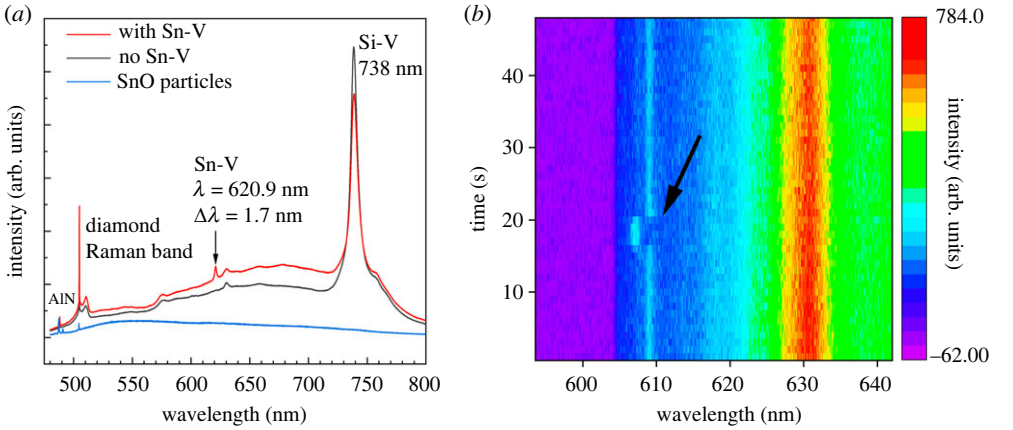

Figure 4. (*a*) PL spectra at room temperature of the as-grown: diamond microcrystals with Sn-V centres (top red curve); diamond microcrystals without Sn-V peaks (black curve), and remaining SnO particles (bottom blue curve). (*b*) Fluorescent track of one of the microcrystals showing pronounced spectral jump.

(b) Raman and photoluminescence spectra at room temperature

The phase composition of the diamond crystallites after acid treatment was studied at RT using Raman spectroscopy (figure 3). The spectra reveal the following features common for CVD-grown diamond: the narrow peak of the diamond phase near 1334 cm^{-1}, and the G-peak at 1570 cm^{-1} from graphitic carbon [42]. The set of peaks at 612, 657 and 669 cm^{-1} are attributed to the AlN substrate [43].

The stress in diamond can be estimated from the shift of the Raman peak ($\Delta\nu = \nu - \nu_0$) from its ideal position at $\nu_0 = 1332.5\,cm^{-1}$ as σ (GPa) $= -0.49 \cdot \Delta\nu$ (cm^{-1}) [44,45]. Figure 3*b* shows the statistical data for the diamond Raman peak over 40 different diamond microcrystals. For different crystals, the position of the diamond peak lies in the range 1332.0–1336.5 cm^{-1}, while full width at half-maximum (FWHM) in the range of 6–10 cm^{-1}. The amount of stress in different microcrystals is roughly estimated to vary from +0.25 GPa tensile stress to −1.5 GPa compressive stress.

The PL spectra taken at RT at different locations of a selected sample are shown in figure 4. The remaining SnO particles do not give any contribution to the PL spectra other than Raman peaks in the 490–520 nm region (blue curve). The most intense line in the PL spectra for all microcrystals

was the Si-V peak with ZPL at 738 nm and FWHM of ≈5 nm. Neither the position nor the width of the Si-V peak showed any unusual behaviour from crystal to crystal. On the other hand, the statistical investigation of the grown material shows that only a small portion of microcrystals, estimated at ≈10–15% of the total number, reveals any Sn-V signal observed as a clear PL peak near 620 nm (red curve in figure 4*a*). Most of the microcrystals do not show any signs of Sn-V (black curve in figure 4*a*). The FWHM of the observed Sn-V peaks ranged from 1.1 to 1.7 nm. This is much lower than typical values (approx. 5 nm) for Group-IV centres at RT even in low-stress high-quality single diamond crystals [15,19,21,26,46]. Additionally, this is close to the best value of 1.98 nm obtained in the work [31] for single-crystal diamond sample after Sn ion implantation and low-temperature vacuum annealing at 1200°C.

Another intriguing result is associated with spectral diffusion (figure 4*b*). We observed an example of reversible spectral jumps from 609.1 nm to 607.2 nm of a narrow PL peak (FWHM of ≈1 nm) in one of the microcrystals. We assume that the line can be attributed to the emission of the Sn-V centre even though the wavelength is sufficiently shifted. Spectral diffusion itself proves that the observed line originates from a single emitter because a correlated spectral jump for an ensemble of emitters is highly unlikely. The close location for the emitter to the surface may be the reason of spectral diffusion and possibly the shift of ZPL. The analysis of the second-order cross-correlation function is commonly used to unambiguously verify if the observed PL originates from a single emitter. However, it was not applicable here (at RTs) due to significantly high background fluorescent signal from the diamond particles in relation to the Sn-V emission (see figure 4*a*). Indeed, large contribution of noise signal to single-photon emitter luminescence can mask expected antibunching effect [47]. A reliable way to significantly improve the 'signal-to-noise' ratio is to perform measurements at low temperatures, in which case the single-photon emission prevails over the background luminescence noise, so an antibunching can be expected. However, our low-temperature experimental set-up was not equipped with Hanbury Brown and Twiss scheme and did not allow performing such measurements.

(c) Photoluminescence spectra of Sn-V centres at low temperatures

A series of the PL spectra for the several diamond microcrystals with Sn-V signal is shown in figure 5. Similar to the PL spectra investigation at RT, the low-T (7 K) measurements confirmed the absence of Sn-V signal from the majority of the microcrystals. The peak position for the Sn-V centre varied from crystal to crystal and was measured between ≈605 and ≈630 nm, while its FWHM (≈0.05 nm or ≈40 GHz) was relatively constant for the different crystals (figure 5*a*). The measured linewidths were comparable with the resolution of the spectrometer (approx. 0.033 nm), hence we provide values of FWHM after deconvolution [48]. In addition, some crystals had multiple lines near 620 nm (figure 5*b*), such spectra are rather typical for the diamond implanted with Sn ions but before/without additional HPHT annealing. This effect is attributed to inhomogeneous broadening (e.g. [31,49]). Similar spectra with single or multiple narrow lines were observed for CVD diamond films with Ge-V centres reported elsewhere [50].

4. Discussion

The results in this work clearly highlight the difficulty of incorporation of large atoms like Sn into dense diamond lattice. Despite the abundance of the Sn impurity sources near the growing diamond crystallites, the PL signal from Sn-V centres may be found only in a relatively small number of them. On the other hand, the unintentional Si doping, which had no active sources of impurity other than contamination on the reactor walls, resulted in an intense Si-V peak in PL spectra, that was registered for every diamond crystallite and was an order of magnitude more intense than any registered Sn-V peak near 620 nm. Considering the spectral diffusion that was registered for one of the Sn-V peaks, we attribute the obtained spectra with one narrow line to single Sn-V emitters (figure 5*a*). Spectra with multiple shifted peaks may be crystallites with multiple Sn-V centres (rather than one emitter with two- or four-line fine structure), as both the

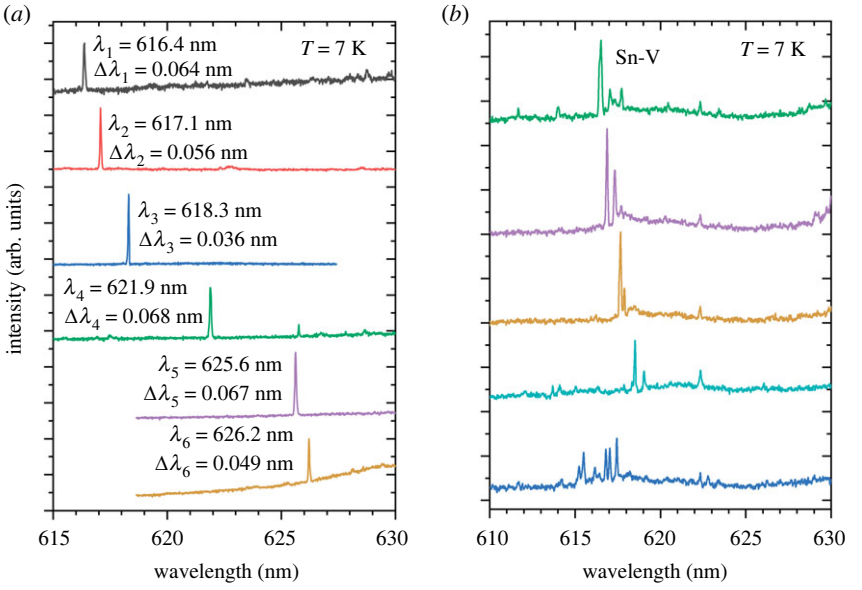

Figure 5. PL spectra of the selected diamond microcrystals: (*a*) a set of spectra with individual Sn-V peaks and (*b*) a set of spectra with multiple Sn-V peaks.

distance and intensity ratio between those peaks are inconsistent and rather random. However, in view of these results, three particular observations need to be addressed: (i) the random shifting of the Sn-V peak position; (ii) the single-line fine structure of the peak at low temperatures; and (iii) the unusually small width of the peak at RT.

(a) Sn-V peak shifts

For Group-IV colour centres in diamond, specifically for well-investigated Si-V and Ge-V, typical four-line fine structure of ZPL can be resolved at low temperatures [21,23,51,52]. A similar picture is observed for Sn-V centres, but a bigger split of the ground state leads to a lower Bolzman population of the upper level of excited state, and therefore ZPL quartet reduces to a doublet at liquid-helium temperatures [15,22,28]. However, the exact fine structure for Sn-V centres at low temperatures does not necessarily show a two-level structure and varies in the literature [15,22,31,53]. In the case of monocrystals, the majority of defects that induce internal stress are 'healed' either during the HPHT process itself or by additional annealing. The shift of the Sn-V peak position in our samples may be explained by the random stress in the environment of the centre. It was shown before that the PL peaks of Group-IV centres shift under high-pressure conditions. The exact shift values for Ge-V and Sn-V centres are an order-of-magnitude higher than that for Si-V centres [54]. So, although for Si-V centres this effect may be neglected, for Ge-V centres such a random shift in the peak position has already been reported [55]. The observed values of tensile/compressive stress of +0.25 to −1.5 GPa imply that the possible spectral shift may reach up to ≈10 nm. Another factor that could potentially influence the position of the Sn-V peak is the isotopic shift [56], however, in the case of Sn isotopes the shift values are expected to be much smaller than for Si and Ge [53].

(b) Single-line fine structure

As it was mentioned before, the typical fine structure of any Group-IV centre at low temperatures usually consists of four narrow lines, which represent four possible transitions between two split

ground states and two split excited states [51]. Such shape of the spectrum, however, normally is characteristic for the most high-quality and stress-free single crystals [46,56]. The excessive number of defects together with the high values of the stress in the film leads to the merging of those four lines to a single broad peak (see [26]). For Si-V centres, an increase in stress leads to a change in the relative intensity and position of those four components. First demonstration of this effect was done in a dissertation by Hepp [57] (see fig. 5.2 on p. 164), where it was shown that the compressive stress applied to Si-doped diamond (less than 0.4 GPa) changes the four-line fine structure of Si-V centres. Similar results were obtained in the work by Meesala *et al*. [58], where stress was deliberately and controllably applied to Si-V centres in order to affect the spectrum at low temperatures. In both works, it was shown that if sufficient stress is applied to the Si-V centre, the one-line fine structure can be obtained, with the other three lines being weak and distanced from the main line. Moreover, according to works [53,54], the PL behaviour of Sn-V centres is even more sensitive to stress, so a single-line thin structure is well-expected even for relatively low values of stress revealed for diamond microcrystals in the current study.

For some crystals, we also observed the PL spectra with multiple narrowband lines (figure 5*b*). This type of spectra was reported by Iwasaki *et al.* [15] to be characteristic of Sn-V centre ensemble at low temperatures if HPHT annealing is not performed in Sn-implanted high-quality single-crystal diamond. Thus, in our study, the multiple narrow line structure may be attributed to a small ensemble of randomly shifted narrowband Sn-V centres in one diamond crystallite. We see that stresses are inhomogeneous within one crystallite, and the variation of stresses inside one crystal may be even bigger than the variation between different crystals (FWHM of the Raman line is much bigger than shifts between various crystals).

(c) The linewidth of Sn-V at room temperature

The observation of narrowband (FWHM 1.1–1.7 nm) luminescence and spectral diffusion at RTs are the most interesting and unexpected findings of this work. Slightly larger values for FWHM(Sn-V) = 1.98 nm were reported by Görlitz *et al*. [31] for the diamond single-crystal implanted with Sn ions followed by vacuum annealing at 1200°C. Interestingly, the sample annealed under HPHT conditions (thus, less defective and with smaller values of residual stress) had a much broader PL peak with FWHM(Sn-V) = 6.15 nm at RT, while still demonstrating a two-line fine structure at T = 10 K. Moreover, the low-temperature PL spectrum of the vacuum-annealed sample (fig. 7*b* in [31]) is rather similar to the spectra shown in figure 5*b* with a set of narrow Sn-V peaks. The observed peaks showed a random distribution of their intensities and positions. The high concentration of Sn-V centres made it difficult to observe separate Sn-V lines from single centres in [31]. However, combined with our results, we hypothesize that Sn-V centres in a diamond under stress experience a sufficient shift in the typical four-level energy structure of Group-IV colour centres. This results in the change of its PL behaviour both at low and RT. The variations in Sn-V peak shift and broadening may be influenced not only by the absolute values of the strain but also by variation of ratio between longitudinal strain and transverse strain [59] even if the strain magnitude is constant. Recently, Meesala *et al*. [58] demonstrated the control over the electronic structure of Si-V centres with stress/strain by using a laboratory-built nano-electro-mechanical system. Following their logic, we suggest that the control over strain/stress of diamond with Group-IV centres can be efficiently used to fine-tune diamond-based quantum devices and also to control the luminescent properties of diamond in general.

5. Conclusion

In this work, we presented the fabrication of a luminescent Sn-doped diamond using microwave plasma-assisted CVD in methane–hydrogen gas mixtures. The SnO_2 nanoparticles, which were heated and etched by the plasma, were used as solid-state impurity source. The obtained diamond microcrystals with sizes of 2–4 µm exhibit the PL of Sn-V colour centres near 620 nm. At RT, the measured PL peak position was 620.9 nm, while FWHM was as small as 1.1–1.7 nm. At low

temperatures (7 K), the FWHM of the Sn-V ZPL decreased to ≈0.05 nm (≈40 GHz), while the peak position was randomly shifted. The shift in the peak position is attributed to the random values of stress/strain in different diamond crystals.

The obtained results open the path to formation of luminescent Sn-doped CVD diamond with the potential to improve the characteristics of the resulting material by additional irradiation and/or HPHT annealing. In addition, the narrowing of the Sn-V ZPL, both at low and RTs stimulates a further investigation of the controllably strained/stressed diamond with Group-IV colour centres for a multitude of applications in quantum optics.

Data accessibility. The Raman and PL spectra supporting this article have been uploaded as part of the electronic supplementary material [60].

Declaration of AI use. We have not used AI-assisted technologies in creating this article.

Authors' contributions. V.S.: conceptualization, funding acquisition, project administration, resources, visualization, writing—original draft, writing—review and editing; A.M.: data curation, investigation; A.N.: data curation, investigation, writing—original draft; I.T.: investigation; S.S.: investigation, software, visualization; I.E.: data curation, formal analysis, investigation, writing—original draft; M.E.: investigation; M.P.: investigation; S.M.: formal analysis, validation, writing—original draft, writing—review and editing; V.R.: supervision, writing—original draft, writing—review and editing; A.N.: formal analysis, supervision, validation, writing—original draft, writing—review and editing.

All authors gave final approval for publication and agreed to be held accountable for the work performed therein.

Conflict of interest declaration. We declare we have no competing interests.

Funding. The work was funded by the Russian Science Foundation, grant no. 21-72-10153, https://rscf.ru/project/21-72-10153/.

Acknowledgements. The authors would like to thank Christoph Becher for the helpful discussions, and Dmitry Yakovlev and Alexey Popovich for their help with the preparation of the SnO_2 precursors.

References

1. Iwasaki T. 2020 Color centers based on heavy group-IV elements. In *Semiconductors and semimetals* (eds CE Nebel, I Aharonovich, N Mizuochi, M Hatano), pp. 237–256. Elsevier.
2. Bradac C, Gao W, Forneris J, Trusheim ME, Aharonovich I. 2019 Quantum nanophotonics with group IV defects in diamond. *Nat. Commun.* **10**, 1–13. (doi:10.1038/s41467-019-13332-w)
3. Kuruma K, Pingault B, Chia C, Renaud D, Hoffmann P, Iwamoto S, Ronning C, Lončar M. 2021 Coupling of a single tin-vacancy center to a photonic crystal cavity in diamond. *Appl. Phys. Lett.* **118**, 230601. (doi:10.1063/5.0051675)
4. Rugar AE, Aghaeimeibodi S, Riedel D, Dory C, Lu H, Mcquade PJ, Shen Z-X, Melosh NA, Vučković J. 2021 Quantum photonic interface for tin-vacancy centers in diamond. *Phys. Rev. X* **11**, 031021. (doi:10.1103/PhysRevX.11.031021)
5. Ruf M, Wan NH, Choi H, Englund D, Hanson R. 2021 Quantum networks based on color centers in diamond. *J. Appl. Phys.* **130**, 070901. (doi:10.1063/5.0056534)
6. Chen D, Zheludev N, Gao W. 2020 Building blocks for quantum network based on group-IV split-vacancy centers in diamond. *Adv. Quantum Technol.* **3**, 1900069. (doi:10.1002/qute.201900069)
7. Chen X, Zhang W. 2017 Diamond nanostructures for drug delivery, bioimaging, and biosensing. *Chem. Soc. Rev.* **46**, 734–760. (doi:10.1039/C6CS00109B)
8. Chauhan S, Jain N, Nagaich U. 2020 Nanodiamonds with powerful ability for drug delivery and biomedical applications: recent updates on *in vivo* study and patents. *J. Pharm. Anal.* **10**, 1–12. (doi:10.1016/j.jpha.2019.09.003)
9. Nunn N, Shames AI, Torelli M, Smirnov AI, Shenderova O. 2022 Luminescent diamond: a platform for next generation nanoscale optically driven quantum sensors. In *Luminescent nanomaterials* (ed. OM Ntwaeaborwa), pp. 1–95. New York, NY: Jenny Stanford Publishing.
10. Kucsko G, Maurer PC, Yao NY, Kubo M, Noh HJ, Lo PK, Park H, Lukin MD. 2013 Nanometre-scale thermometry in a living cell. *Nature* **500**, 54–58. (doi:10.1038/nature12373)
11. Nguyen CT *et al.* 2018 All-optical nanoscale thermometry with silicon-vacancy centers in diamond. *Appl. Phys. Lett.* **112**, 203102. (doi:10.1063/1.5029904)

12. Alkahtani M, Cojocaru I, Liu X, Herzig T, Meijer J, Küpper J, Lühmann T, Akimov AV, Hemmer PR. 2018 Tin-vacancy in diamonds for luminescent thermometry. *Appl. Phys. Lett.* **112**, 241902. (doi:10.1063/1.5037053)
13. Romshin AM, Zeeb V, Martyanov AK, Kudryavtsev OS, Pasternak DG, Sedov VS, Ralchenko VG, Sinogeykin AG, Vlasov II. 2021 A new approach to precise mapping of local temperature fields in submicrometer aqueous volumes. *Sci. Rep.* **11**, 14228. (doi:10.1038/s41598-021-93374-7)
14. Trusheim ME *et al.* 2020 Transform-limited photons from a coherent tin-vacancy spin in diamond. *Phys. Rev. Lett.* **124**, 023602. (doi:10.1103/PhysRevLett.124.023602)
15. Iwasaki T, Miyamoto Y, Taniguchi T, Siyushev P, Metsch MH, Jelezko F, Hatano M. 2017 Tin-vacancy quantum emitters in diamond. *Phys. Rev. Lett.* **119**, 253601. (doi:10.1103/PhysRevLett.119.253601)
16. Pingault B *et al.* 2014 All-optical formation of coherent dark states of silicon-vacancy spins in diamond. *Phys. Rev. Lett.* **113**, 263601. (doi:10.1103/PhysRevLett.113.263601)
17. Pingault B, Jarausch D-D, Hepp C, Klintberg L, Becker JN, Markham M, Becher C, Atatüre M. 2017 Coherent control of the silicon-vacancy spin in diamond. *Nat. Commun.* **8**, 15579. (doi:10.1038/ncomms15579)
18. Zaitsev AM, Vavilov VS, Gippius AA. 1981 Cathodoluminescence of diamond associated with silicon impurity. *Sov. Phys. Lebedev Inst. Rep.* **10**, 15–17.
19. Iwasaki T *et al.* 2015 Germanium-vacancy single color centers in diamond. *Sci. Rep.* **5**, 12882. (doi:10.1038/srep12882)
20. Ralchenko VG, Sedov VS, Khomich AA, Krivobok VS, Nikolaev SN, Savin SS, Vlasov II, Konov VI. 2015 Observation of the Ge-vacancy color center in microcrystalline diamond films. *Bull. Lebedev Phys. Inst.* **42**, 165–168. (doi:10.3103/S1068335615060020)
21. Ekimov EA, Lyapin SG, Boldyrev KN, Kondrin MV, Khmelnitskiy R, Gavva VA, Kotereva TV, Popova MN. 2015 Germanium–vacancy color center in isotopically enriched diamonds synthesized at high pressures. *JETP Lett.* **102**, 701–706. (doi:10.1134/S0021364015230034)
22. Ekimov EA, Lyapin SG, Kondrin MV. 2018 Tin-vacancy color centers in micro- and polycrystalline diamonds synthesized at high pressures. *Diamond Relat. Mater.* **87**, 223–227. (doi:10.1016/j.diamond.2018.06.014)
23. Palyanov YN, Kupriyanov IN, Borzdov YM, Surovtsev NV. 2015 Germanium: a new catalyst for diamond synthesis and a new optically active impurity in diamond. *Sci. Rep.* **5**, 1–8. (doi:10.1038/srep14789)
24. Van Dam SB *et al.* 2019 Optical coherence of diamond nitrogen-vacancy centers formed by ion implantation and annealing. *Phys. Rev. B* **99**, 161203. (doi:10.1103/PhysRevB.99.161203)
25. Uzan-Saguy C, Cytermann C, Brener R, Richter V, Shaanan M, Kalish R. 1995 Damage threshold for ion-beam induced graphitization of diamond. *Appl. Phys. Lett.* **67**, 1194–1196. (doi:10.1063/1.115004)
26. Sedov V *et al.* 2018 Growth of polycrystalline and single-crystal CVD diamonds with bright photoluminescence of Ge-V color centers using germane GeH4 as the dopant source. *Diamond Relat. Mater.* **90**, 47–53. (doi:10.1016/j.diamond.2018.10.001)
27. Sedov VS *et al.* 2022 Formation of germanium–vacancy color centers in CVD diamond. *J. Russ. Laser Res.* **43**, 1–6. (doi:10.1007/s10946-022-10076-9)
28. Palyanov YN, Kupriyanov IN, Borzdov YM. 2019 High-pressure synthesis and characterization of Sn-doped single crystal diamond. *Carbon* **143**, 769–775. (doi:10.1021/acsami.0c07242)
29. Westerhausen MT, Trycz AT, Stewart C, Nonahal M, Regan B, Kianinia M, Aharonovich I. 2020 Controlled doping of GeV and SnV color centers in diamond using chemical vapor deposition. *ACS Appl. Mater. Interfaces* **12**, 29 700–29 705. (doi:10.1021/acsami.0c07242)
30. Lühmann T, Küpper J, Dietel S, Staacke R, Meijer J, Pezzagna S. 2020 Charge-state tuning of single SnV centers in diamond. *ACS Photonics* **7**, 3376–3385. (doi:10.1021/acsphotonics.0c01123)
31. Görlitz J *et al.* 2020 Spectroscopic investigations of negatively charged tin-vacancy centres in diamond. *New J. Phys.* **22**, 013048. (doi:10.1088/1367-2630/ab6631)
32. Rugar AE, Lu H, Dory C, Sun S, Mcquade PJ, Shen Z-X, Melosh NA, Vučković J. 2020 Generation of tin-vacancy centers in diamond via shallow ion implantation and subsequent diamond overgrowth. *Nano Lett.* **20**, 1614–1619. (doi:10.1021/acs.nanolett.9b04495)

33. Debroux R *et al.* 2021 Quantum control of the tin-vacancy spin qubit in diamond. *Phys. Rev. X* **11**, 041041. (doi:10.1103/PhysRevX.11.041041)
34. Sedov VS, Vlasov II, Ralchenko VG, Khomich AA, Konov VI, Fabbri AG, Conte G. 2011 Gas-phase growth of silicon-doped luminescent diamond films and isolated nanocrystals. *Bull. Lebedev Phys. Inst.* **38**, 291–296. (doi:10.3103/S1068335611100034)
35. Sedov V *et al.* 2020 Effect of substrate holder design on stress and uniformity of large-area polycrystalline diamond films grown by microwave plasma-assisted CVD. *Coatings* **10**, 939. (doi:10.3390/coatings10100939)
36. Sedov VS, Martyanov AK, Khomich AA, Savin SS, Zavedeev EV, Ralchenko VG. 2020 Deposition of diamond films on Si by microwave plasma CVD in varied CH_4-H_2 mixtures: reverse nanocrystalline-to-microcrystalline structure transition at very high methane concentrations. *Diamond Relat. Mater.* **109**, 108072. (doi:10.1016/j.diamond.2020.108072)
37. Vlasov II, Barnard AS, Ralchenko VG, Lebedev OI, Kanzyuba MV, Saveliev AV, Konov VI, Goovaerts E. 2009 Nanodiamond photoemitters based on strong narrow-band luminescence from silicon-vacancy defects. *Adv. Mater.* **21**, 808–812. (doi:10.1002/adma.200802160)
38. Pasternak DG, Dai J, Kalashnikov DA, Sedov VS, Martyanov AK, Ralchenko VG, Krivitsky LA, Vlasov II. 2020 Low-Temperature silicon-vacancy luminescence of individual chemical vapor deposition nanodiamonds grown by seeding and spontaneous nucleation. *Phys. Status Solidi (a)* **218**, 2000274. (doi:10.1002/pssa.202000274)
39. Sedov V, Martyanov A, Popovich A, Savin S, Sovyk D, Tiazhelov I, Pasternak D, Mandal S, Ralchenko V. 2023 Microporous poly-and monocrystalline diamond films produced from chemical vapor deposited diamond–germanium composites. *Nanoscale Adv.* **5**, 1307–1315. (doi:10.1039/D2NA00688J)
40. Zhang G, Liu N, Ren Z, Yang B. 2011 Synthesis of high-purity SnO_2 nanobelts by using exothermic reaction. *J. Nanomater.* **2011**, 1–5. (doi:10.1155/2011/526094)
41. Guo XW, Fang XP, Sun Y, Shen LY, Wang ZX, Chen LQ. 2013 Lithium storage in carbon-coated SnO_2 by conversion reaction. *J. Power Sources* **226**, 75–81. (doi:10.1016/j.jpowsour.2012.10.068)
42. Vlasov II, Goovaerts E, Ralchenko VG, Konov VI, Khomich AV, Kanzyuba MV. 2007 Vibrational properties of nitrogen-doped ultrananocrystalline diamond films grown by microwave plasma CVD. *Diamond Relat. Mater.* **16**, 2074–2077. (doi:10.1016/j.diamond.2007.07.007)
43. Cao YG, Chen XL, Lan YC, Li JY, Xu YP, Xu T, Liu QL, Liang JK. 2000 Blue emission and Raman scattering spectrum from AlN nanocrystalline powders. *J. Cryst. Growth* **213**, 198–202. (doi:10.1016/S0022-0248(00)00379-1)
44. Ager JW. 1995 Residual stress in diamond and amorphous carbon films. *MRS Online Proc. Libr. Arch.* **383**, 143. (doi:10.1557/PROC-383-143)
45. Mandal S, Arts K, Knoops HC, Cuenca JA, Klemencic GM, Williams OA. 2021 Surface zeta potential and diamond growth on gallium oxide single crystal. *Carbon* **181**, 79–86. (doi:10.1016/j.carbon.2021.04.100)
46. Bolshakov A *et al.* 2015 Photoluminescence of SiV centers in single crystal CVD diamond *in situ* doped with Si from silane. *Phys. Status Solidi (a)* **212**, 2525–2532. (doi:10.1002/pssa.201532174)
47. Eremchev IY, Tarasevich AO, Li J, Naumov AV, Scheblykin IG. 2021 Lack of photon antibunching supports supertrap model of photoluminescence blinking in Perovskite sub-micrometer crystals. *Adv. Opt. Mater.* **9**, 2001596. (doi:10.1002/adom.202001596)
48. Rautian SG. 1958 Real spectral apparatus. *Sov. Phys. Uspekhi* **1**, 245. (doi:10.1070/PU1958v001n02ABEH003099)
49. Rugar AE, Dory C, Aghaeimeibodi S, Lu H, Sun S, Mishra SD, Shen Z-X, Melosh NA, Vuckovic J. 2020 Narrow-linewidth tin-vacancy centers in a diamond waveguide. *ACS Photonics* **7**, 2356–2361. (doi:10.1021/acsphotonics.0c00833)
50. Eremchev IY, Neliubov AY, Boldyrev KN, Ralchenko VG, Sedov VS, Kador L, Naumov AV. 2021 Microscopic insight into the inhomogeneous broadening of zero-phonon lines of GeV–color centers in chemical vapor deposition diamond films synthesized from gaseous germane. *J. Phys. Chem. C* **125**, 17 774–17 785. (doi:10.1021/acs.jpcc.1c02617)
51. Dietrich A, Jahnke KD, Binder JM, Teraji T, Isoya J, Rogers LJ, Jelezko F. 2014 Isotopically varying spectral features of silicon-vacancy in diamond. *New J. Phys.* **16**, 113019. (doi:10.1088/1367-2630/16/11/113019)

52. Sedov V, Boldyrev K, Krivobok V, Nikolaev S, Bolshakov A, Khomich A, Khomich A, Krasilnikov A, Ralchenko V. 2017 SiV color centers in Si-doped isotopically enriched 12C and 13C CVD diamonds. *Phys. Status Solidi (a)* **214**, 1700198. (doi:10.1002/pssa.201700198)
53. Narita Y, Wang P, Ikeda K, Oba K, Miyamoto Y, Taniguchi T, Onoda S, Hatano M, Iwasaki T. 2023 Multiple tin-vacancy centers in diamond with nearly identical photon frequency and linewidth. *Phys. Rev. Appl.* **19**, 024061. (doi:10.1103/PhysRevApplied.19.024061)
54. Vindolet B *et al.* 2022 Optical properties of SiV and GeV color centers in nanodiamonds under hydrostatic pressures up to 180 GPa. *Phys. Rev. B* **106**, 214109. (doi:10.1103/PhysRevB.106.214109)
55. Mary Joy R *et al.* 2023 Germanium vacancy centre formation in CVD nanocrystalline diamond using a solid dopant source. *Sci. Talks* **5**, 100157. (doi:10.1016/j.sctalk.2023.100157)
56. Ralchenko VG *et al.* 2018 Monoisotopic ensembles of silicon-vacancy color centers with narrow-line luminescence in homoepitaxial diamond layers grown in H_2–CH_4–$^{x}SiH_4$ gas mixtures ($x = 28, 29, 30$). *ACS Photonics* **6**, 66–72. (doi:10.1021/acsphotonics.8b01464)
57. Hepp C. 2014 Electronic structure of the silicon vacancy color center in diamond. Doctoral thesis.
58. Meesala S *et al.* 2018 Strain engineering of the silicon-vacancy center in diamond. *Phys. Rev. B* **97**, 205444. (doi:10.1103/PhysRevB.97.205444)
59. Lang J, Häußler S, Fuhrmann J, Waltrich R, Laddha S, Scharpf J, Kubanek A, Naydenov B, Jelezko F. 2020 Long optical coherence times of shallow-implanted, negatively charged silicon vacancy centers in diamond. *Appl. Phys. Lett.* **116**, 064001. (doi:10.1063/1.5143014)
60. Sedov V *et al.* 2023 Narrowband photoluminescence of Tin-Vacancy colour centres in Sn-doped chemical vapour deposition diamond microcrystals. Figshare. (doi:10.6084/m9.figshare.c.6908883)